

# Quantitation of DNA double-strand break resection intermediates in human cells

Yi Zhou<sup>1,2</sup>, Pierre Caron<sup>3,4</sup>, Gaëlle Legube<sup>3,4</sup> and Tanya T. Paull<sup>1,2,\*</sup>

<sup>1</sup>The Department of Molecular Biosciences, The Howard Hughes Medical Institute, The University of Texas at Austin, Austin, TX 78712, USA, <sup>2</sup>Institute for Cellular and Molecular Biology, The University of Texas at Austin, Austin, TX 78712, USA, <sup>3</sup>Université de Toulouse, UPS, LBCMCP, 31062 Toulouse, France and <sup>4</sup>CNRS, LBCMCP, F-31062 Toulouse, France

Received September 11, 2013; Revised November 24, 2013; Accepted November 25, 2013

## ABSTRACT

**5' strand resection at DNA double strand breaks (DSBs) is critical for homologous recombination (HR) and genomic stability. Here we develop a novel method to quantitatively measure single-stranded DNA intermediates in human cells and find that the 5' strand at endonuclease-generated break sites is resected up to 3.5kb in a cell cycle-dependent manner. Depletion of CtIP, Mre11, Exo1 or SOSS1 blocks resection, while depletion of 53BP1, Ku or DNA-dependent protein kinase catalytic subunit leads to increased resection as measured by this method. While 53BP1 negatively regulates DNA end processing, depletion of Brca1 does not, suggesting that the role of Brca1 in HR is primarily to promote Rad51 filament formation, not to regulate end resection.**

## INTRODUCTION

DNA double strand breaks (DSBs) are one of the most deleterious types of DNA damage that can lead to chromosome rearrangements, genomic instability and tumorigenesis if not repaired correctly (1). Nonhomologous end joining (NHEJ) and homologous recombination (HR) are the two major DSB repair pathways in eukaryotic cells. NHEJ is the primary pathway and is used throughout the cell cycle, while HR is active in S and G<sub>2</sub> phases where sister chromatids are available as repair templates (2). HR is initiated with the resection of the 5' strands to generate 3' single-stranded DNA (ssDNA), which is required for Rad51 binding and strand invasion. Therefore, the initiation of resection is thought to be a critical control point for the choice between HR and NHEJ because this process commits the breaks to HR repair.

The proteins required for 5' strand resection at DSBs in eukaryotic cells include the Mre11/Rad50/Nbs1 (MRN)

complex, which binds to DSBs and promotes resection by two independent endo/exonucleases: Exo1 and Dna2 (3). The CtIP protein also participates in this process and promotes long-range resection in conjunction with MRN (4). The Ataxia-Telangiectasia-Mutated (ATM) protein kinase has also been shown to be required for DSB resection (5–7) although its role in this process is not completely understood.

The Ku70/80 heterodimer and DNA-dependent protein kinase catalytic subunit (DNA-PKcs) coordinate the process of NHEJ. After binding of Ku and subsequent recruitment of DNA-PKcs to DSBs, an active DNA-PK holoenzyme is formed that mediates the phosphorylation of DNA-PKcs itself as well as other NHEJ factors (8). Autophosphorylated DNA-PKcs undergoes a large conformational change that is thought to promote its dissociation from DNA ends and facilitate end joining (9–13). Residues T2609 and T2647 in the ABCDE cluster are DNA-PKcs autophosphorylation sites (14) but have also been shown to be targets of ATM (15). Apart from its role in NHEJ, DNA-PKcs has also been implicated in regulation of HR (13,16–19), but the underlying mechanism is not fully understood. Previous studies have demonstrated that the human Ku heterodimer inhibits 5' strand resection mediated by Exo1 or Dna2 *in vitro*, while MRN overcomes Ku inhibition of resection (20,21), but it is not clear whether DNA-PKcs also regulates this process.

Currently, DSB resection in mammalian cells is assessed indirectly using RPA foci, Rad51 foci or BrdU detection in ssDNA, all of which are subjectively dependent on the immunofluorescence protocol and antibody used and cannot determine the length of resection from a DSB site. Here we describe an assay to measure levels of ssDNA at specific DSB sites in human cells that is quantitative and precise with respect to the extent and efficiency of resection. Using this method, we find that resection at endonuclease-induced breaks occurs up to 3.5 kb from the break site and is more efficient in S/G<sub>2</sub> phase cells compared with cells in G<sub>1</sub> phase. We also find that the

\*To whom correspondence should be addressed. Tel: +1 512 232 7802; Fax: +1 512 471 3730; Email: tpaull@utexas.edu

MRN complex, Exo1, SOSS1 and CtIP promote the processing DSB ends into ssDNA. In contrast, depletion of Ku, DNA-PKcs or 53BP1 leads to increased ssDNA formation at DSB sites, consistent with the idea that NHEJ factors inhibit resection. Lastly, we find that BRCA1 depletion has little effect on resection, whereas it strongly reduces Rad51 foci, suggesting that the effect of BRCA1 on HR may be specific to Rad51 filament formation, not directly on the processing of DSB ends.

## MATERIALS AND METHODS

### Cell culture, transfection and sorting

ER-*AsiSI* U2OS cells and 293T cells were grown in Dulbecco's Modified Eagle Medium (Gibco) containing 10% fetal bovine serum (FBS; Gibco). Wild type (WT), Ku86 Flox/+, Ku86Flox/- and DNA-PKcs-/- HCT116 cells were provided by Dr Eric Hendrickson and were grown in McCoy' 5A medium (Gibco) supplemented with 10% FBS and 2mM L-glutamine (Gibco). siRNA transfection in ER-*AsiSI* U2OS cells was performed using Lipofectamine 2000 (Invitrogen) following manufacturer's instructions. For purification of G<sub>1</sub> and S/G<sub>2</sub>/M ER-*AsiSI* 293T cells using the FUCCI system (22), 15 µg of pRetroX-G<sub>1</sub>-Red vector and 15 µg of pRetroX-SG<sub>2</sub>M-Cyan vectors (Clontech) were co-transfected into 70% confluent ER-*AsiSI* 293T cells in 15-cm dishes using 40 µl of 1mg/ml Polyethyleneimine (Polysciences). Ten dishes of transfected cells were harvested and subjected to cell sorting using BD FACSAria (BD Biosciences) 24h after transfection. To analyze cell cycle, cells were fixed with 100% cold ethanol, stained with propidium iodide (PI; Sigma) and subjected to flow cytometric analysis.

### Reagents, antibodies and western blotting

4-Hydroxytamoxifen (4-OHT) was purchased from Sigma (catalog no. H7904). Antibodies for western blotting: PARP-1 (Genetex, GTX75098), CtIP (Active Motif, 61141), Mre11 (Genetex, GTX70212), SSB1 (Bethyl, A301-938A), Exo1 (Genetex, GTX109891), BRCA1 (Santa Cruz, sc-6954), 53BP1 (Cell Signaling, 4937), DNA-PKcs (Abcam, ab1832), HA Tag (Bethyl, A190-108A), phospho-(Ser) CDKs substrate (Cell Signaling, 2324), Ku86 (Santa Cruz, sc-5280), RPA (Genetex, GTX22175) and custom RAD51 antibody.

For western blotting analysis, cells were lysed in Laemmli lysis buffer [10% glycerol, 2% (m/v) sodium dodecyl sulphate (SDS), 64mM Tris-HCl, pH 6.8], boiled for 5 min and sonicated. Protein concentrations were measured using BCA protein assay kit (Pierce). Cell lysates were mixed with 5× SDS loading buffer and boiled for 5 min. Proteins were separated by 6–12% SDS-polyacrylamide gel electrophoresis, transferred to PVDF-FL membrane (Millipore) and probed with primary antibodies listed above, followed by detection with IRdye 800 anti-mouse (Rockland, RL-610-132-121) or AlexaFluor 680 anti-rabbit (Invitrogen, A21076) secondary antibodies. Membranes were scanned using a Licor Odyssey scanner.

### Immunostaining

Cells were fixed with 4% formaldehyde for 20 min, followed by permeabilization with cold methanol for 5 min, blocking with 8% bovine serum albumin for 1 h, incubation with primary antibodies for 1 h and secondary antibodies (donkey anti-rabbit IgG Alexa Fluor 594 and donkey anti-mouse IgG Alexa Fluor 488 from Invitrogen) for 30 min at room temperature. For RPA staining, cells were pre-extracted with a buffer containing 20 mM Hepes (pH 7.5), 50 mM NaCl, 3 mM MgCl<sub>2</sub>, 300 mM Sucrose and 0.5% Triton X-100 for 5 min on ice before fixation. For RAD51 staining, this step was performed after methanol permeabilization.

### Genomic DNA extraction

ER-*AsiSI* U2OS cells were trypsinized, centrifuged and resuspended with 37°C 0.6% low-gelling point agarose (BD Biosciences) in PBS (Gibco) at a concentration of 6 × 10<sup>6</sup> cells/ml (For gDNA extraction in ER-*AsiSI* HCT116 cells and ER-*AsiSI* 293T cells, the concentration is 1.5 × 10<sup>6</sup> cells/ml). A 50-µl cell suspension was dropped on a piece of Parafilm (Pechiney) to generate a solidified agar ball, which was then transferred to a 1.5-ml Eppendorf tube. The agar ball was treated with 1 ml of ESP buffer (0.5 M EDTA, 2% N-lauroylsarcosine, 1 mg/ml proteinase-K, 1 mM CaCl<sub>2</sub>, pH 8.0) for 20 h at 16°C with rotation, followed by treatment with 1 ml of HS buffer (1.85 M NaCl, 0.15 M KCl, 5 mM MgCl<sub>2</sub>, 2 mM EDTA, 4 mM Tris, 0.5% Triton X-100, pH 7.5) for 20 h at 16°C with rotation. After washing with 1 ml of phosphate buffer (8 mM Na<sub>2</sub>HPO<sub>4</sub>, 1.5 mM KH<sub>2</sub>PO<sub>4</sub>, 133 mM KCl, 0.8 mM MgCl<sub>2</sub>, pH 7.4) for 6 × 1 h at 4°C with rotation, the agar ball was melted by placing the tube in a 70°C heat block for 10 min. The melted sample was diluted 15-fold with 70°C ddH<sub>2</sub>O, mixed with equal volume of appropriate 2× NEB restriction enzyme buffer and stored at 4°C for future use.

### Measurement of resection in mammalian cells

The level of resection adjacent to specific DSBs was measured by quantitative polymerase chain reaction (qPCR) using a modification of the original yeast method (23). The sequences of qPCR primers and probes are shown in Supplementary Table S2. Twenty microliters of genomic DNA sample (~140 ng in 1× NEB restriction enzyme buffer 4) was digested or mock digested with 20 units of restriction enzymes (BsrGI, BamHI-HF or HindIII-HF; New England Biolabs) at 37°C overnight. Three microliters of digested or mock-digested samples (~20 ng) were used as templates in 25 µl of qPCR reaction containing 12.5 µl of 2× Taqman Universal PCR Master Mix (ABI), 0.5 µM of each primer and 0.2 µM probe using a ViiA<sup>TM</sup> 7 Real-Time PCR System (ABI). The percentage of ssDNA (ssDNA%) generated by resection at selected sites was determined as previously described (24). Briefly, for each sample, a ΔCt was calculated by subtracting the Ct value of the mock-digested sample from the Ct value of the digested sample. The ssDNA% was calculated with the following equation: ssDNA% = 1/(2<sup>ΔCt</sup> - 1) + 0.5 \* 100 (23).

### ER-AsiSI retrovirus packing and infection

ER-AsiSI retrovirus was generated in 293T cells cultured in six-well plates. For each well, 2 µg of pBABE-ER-AsiSI vector was co-transfected with two helper plasmids [1.8 µg of pCS2-mGP (25) and 0.2 µg of pMD2G (D. Trono, Addgene plasmid 12259)] into 95% confluent 293T cells. The cells were split into 6-cm dish 24 h after transfection. Supernatant containing retrovirus was collected and filtered with 0.45 µm syringe filter at 48 and 72 h. The supernatant was aliquoted and stored at -80°C for future use. For ER-AsiSI virus infection, WT, Ku86 Flox/+, Ku86 Flox/−, DNA-PKcs−/− HCT116 cells and 293T cells were grown to ~50% confluency. The cells were cultured with virus-containing supernatant supplemented with 10 µg/ml polybrene (Fisher) overnight. Forty-eight hours after infection, the cells were selected with 2 µg/ml puromycin (Clontech) for ~3 weeks to generate stable cell lines. To delete one allele of Ku86 from Ku86 Flox/+, Ku86 Flox/− cells, the cells were treated with Cre Adenovirus (Vectorbiolabs) for 6 days.

### RNA interference

Ku86 siRNA used in this study was purchased from Qiagen (catalog no. SI2663773). All other siRNAs were purchased from Eurofins MWG Operon. siRNA sequences are as follows: siControl: AAUUCUCCGAAC GUGUCACG UdTdT (26); siCtIP: GCUAAAACAGG AACGAAUCdTdT (4); siMre11: ACAGGAGAAGAG AUCAACUdTdT (26); siSOSS-A: CGUGAUGGCAUG AAUAUUGdTdT (27); siExo1: UAGUGUUUCAGGA UCAACAUCAUCUdTdT (28); siDNA-PKcs: CUUUA UGGUGGCCAUGGAGdTdT (29); siBRCA1: GGAAC CUGUCTCCACAAAGdTdT (30); si53BP1: GGACUC CAGUGUUGUCAUdTdT (31). The efficiency of gene knockdown was examined by western blotting and DSB resection was measured 48 h after transfection.

### Chromatin immunoprecipitation assay

Chromatin immunoprecipitation (ChIP) assays were carried out according to a previously described protocol (32) with the following modifications. Two hundred micrograms of chromatin was immunoprecipitated by using 2 µg of phospho-DNA-PKcs S2056 antibody (Abcam), or no antibody. Immunoprecipitated DNA and input DNA were analyzed in triplicate by qPCR (primer sequences are as follows: DSB1\_FW: GATTGG CTATGGGTGTGGAC, DSB1\_REV: CATCCTTGCA AACCAGTCCT; DSB2\_FW: TTCCTGCAGCCTCATT TTCT, DSB2\_REV: TGATGATGCCTTTTCCCTTC). IP efficiency was calculated as percent of input DNA immunoprecipitated.

## RESULTS

### Development of a quantitative resection assay using the ER-AsiSI system

To quantitate ssDNA at sites of DSBs, we used the ER-AsiSI system in which the restriction enzyme AsiSI is fused to the estrogen receptor hormone-binding domain

(32). The AsiSI enzyme can be induced to enter the nucleus and generate DSBs at sequence-specific sites (5'-GCGATCGC-3') on treatment of the cells with 4-OHT. The genomic DNA was extracted using a method modified from a previously described strategy (33) in which cells are embedded in low-gelling point agar that protects the DNA from shearing and damage during extraction.

To measure resection adjacent to specific DSBs, we chose two AsiSI sites on Chromosome 1 ('DSB1', Chr 1: 89231183; 'DSB2', Chr 1: 109838221) that have been shown to be cleaved with high efficiency (32,34). Three pairs of quantitative PCR (qPCR) primers were designed across BsrGI or BamHI restriction sites at various distances from each AsiSI site (Figure 1A). The restriction enzymes are specific for duplex DNA, thus can be used to distinguish between single-stranded and double-stranded DNA, as demonstrated previously in budding yeast (23). Another two pairs of primers were designed across the two AsiSI sites to monitor the percentage of double strand breaks (DSB%) present at the two sites, as well as a pair of primers at a site where there is no nearby AsiSI sequence on Chromosome 22 ('No DSB'), which was used as a negative control (Figure 1A and Supplementary Figure S1A). The ssDNA% generated by resection at various sites was measured by qPCR as described (24) (see 'Materials and Methods' section for details). Using this method, an increase in ssDNA on 4-OHT treatment was observed adjacent to both DSB sites but not at the site lacking an AsiSI sequence in U2OS cells (Figure 1B). More ssDNA was observed at sites closer to DSBs and the extent of resection was as far as 3500 nucleotides from the DSB end (Figure 1B), with higher levels of resection observed after longer 4-OHT treatment (Figure 1C). Using primers spanning the AsiSI sequence, it was determined that the percentage of DNA cleaved at the DSB1 and DSB2 sites was 21.0 and 8.8%, respectively, after 4 h of 4-OHT exposure (Figure 1D). Considering the levels of ssDNA generated at ~350 nt from DSB1 and DSB2 are ~4 and 2%, we conclude that ~20–26% of DNA ends are actually resected to an extent of 350 nt at both the DSB sites in asynchronously growing U2OS cells (Figure 1D). This may be a low estimate because rapidly repaired breaks would not be detected, but it can be used to estimate the efficiency of DSB resection at sites that are cut and not immediately religated.

### Resection of DSBs is more efficient in S/G<sub>2</sub> phases of the cell cycle

Previous studies showed that DSB resection is cell cycle dependent and preferentially occurs in S and G<sub>2</sub> phases due to a requirement for cyclin-dependent kinase (CDK) activity (2). To test this using the resection assay, we used CDK inhibitor roscovitine (CDKi) to inhibit CDK activity in the asynchronous ER-AsiSI U2OS cell culture (Supplementary Figure S2A) and found that resection efficiency was reduced by roscovitine in a dose-dependent manner (Figure 2A, DSB% in Supplementary Table S1). Roscovitine treatment slightly increased the percentage of cells in G<sub>1</sub> phase (Supplementary Figure

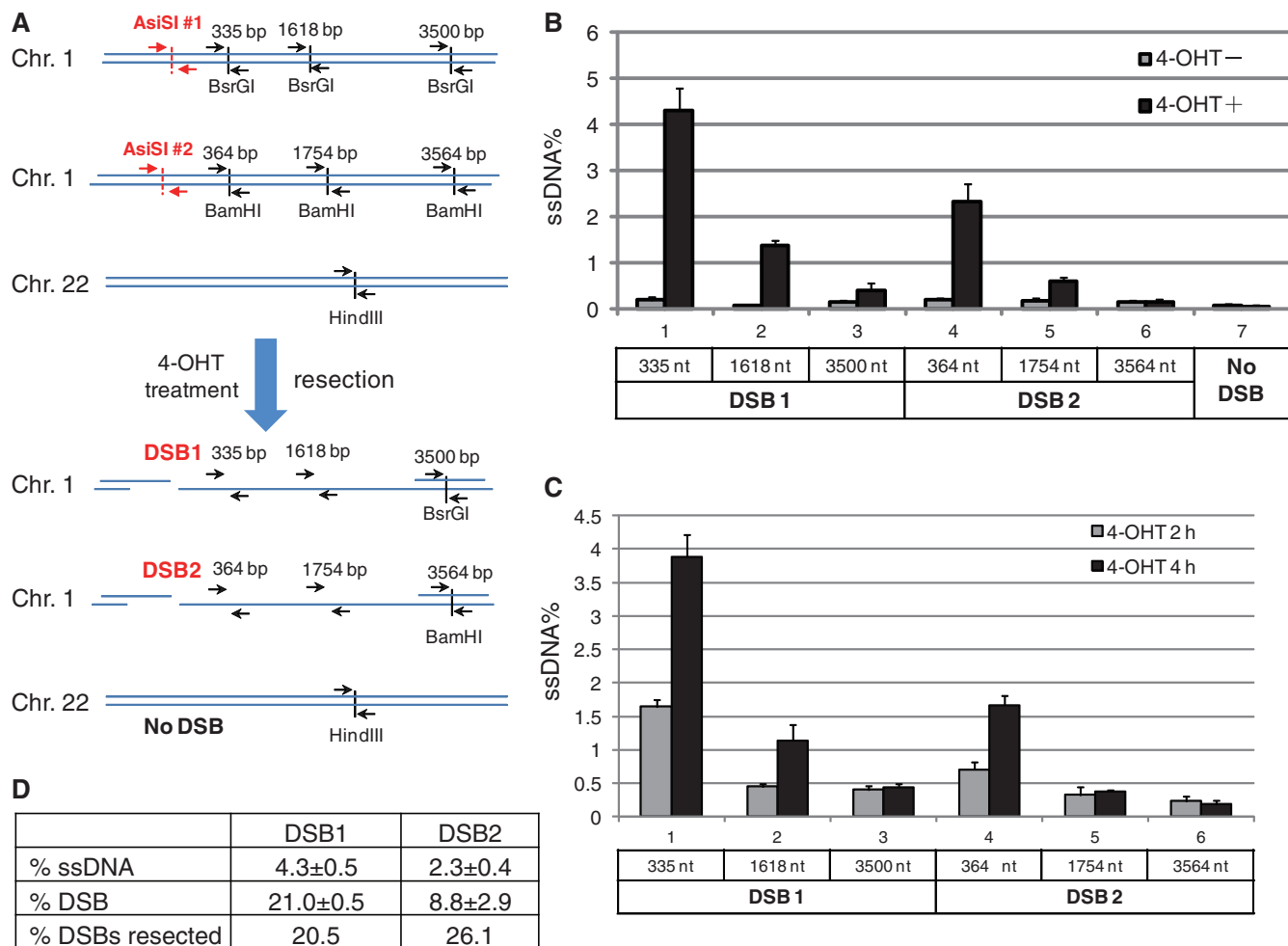


**Figure 1.** Development of a quantitative DNA resection assay in human cells using the ER-*AsiSI* system. (A) Design of Taqman qPCR primers and probes for measurement of DSB% at two *AsiSI* sites (red arrows: DSB1 and DSB2) located on Chromosome 1 and measurement of resection at sites adjacent to the *AsiSI* sites (black arrows). The primers on Chromosome 22 ('No DSB') were used as negative control. The primer pairs for 'DSB1' and 'DSB2' are across *BsrGI* and *BamHI* restriction sites, respectively. The primer pair for 'No DSB' is across a *HindIII* restriction site. All Taqman probes are designed at either side of the restriction site and are not shown in the diagram. (B) ER-*AsiSI* U2OS cells were treated with 300 nM 4-OHT for 4 h or mock treated, genomic DNA (gDNA) was extracted and digested or mock digested with *BsrGI*, *BamHI* or *HindIII* overnight. DNA end resection adjacent to DSB1, DSB2 and No DSB site was measured by qPCR as described in 'Materials and Methods' section. The result is an average of three experiments with error bars showing standard deviation. (C) ER-*AsiSI*-U2OS cells were treated with 300 nM 4-OHT for 2 or 4 h, followed by genomic DNA extraction and measurement of resection as in (B). The result is an average of three experiments with error bars showing standard deviation. (D) Summary of the % ssDNA at DSB1 and DSB2, % DSBs, and the % DSBs resected (% ssDNA/%DSB) at the two selected *AsiSI* sites after 4 h of 4-OHT treatment. % DSB values were measured by qPCR using undigested gDNA samples from B and two sets of primers across the two *AsiSI* sites. The 'No DSB' primers were used to normalize the amount of gDNA in the qPCR reaction. DSB percentages at DSB1 and DSB2 sites in mock-treated cells were both set to zero.

S2B), consistent with the reported function of roscovitine in  $G_1$  arrest (35).

We also used the FUCCI system (22) for selection of cells in either  $G_1$  or S/ $G_2$  phases of the cell cycle in 293T cells stably expressing ER-*AsiSI* (Supplementary Figure S3A and B). Flow cytometry with PI staining was used to determine the percentage of cells in  $G_1$ , S and  $G_2$ (/M) and cell size was also measured. The results confirmed that cells expressing mCherry-Cdt (Red) fluorescent protein were almost exclusively in  $G_1$  phase, while cells expressing AmCyan-Geminin (Green) fluorescent protein were predominantly in the S/ $G_2$ (/M) phases (Figure 2B). As expected, the  $G_1$ -Red cell populations were substantially smaller in size than the S/ $G_2$ (/M)-Green cell populations

(Supplementary Figure S3C), further confirming the accuracy of the FUCCI-based cell sorting. ssDNA at DSB1 and DSB2 was measured in the  $G_1$ -Red cells and the S/ $G_2$ (/M)-Green cells, and compared with that of cells growing asynchronously (unsorted cells) (Figure 2C, DSB% in Supplementary Table S1). Higher levels of resection were observed in cells in S/ $G_2$ (/M) phase compared with the asynchronous culture, and resection was strongly decreased in  $G_1$  cells, consistent with the observed effects of roscovitine. Low levels of resection were still observed in  $G_1$  cells, however, suggesting that end processing does take place inefficiently and results in shorter resection tracks in  $G_1$  cells compared with cells in S or  $G_2$  phase.

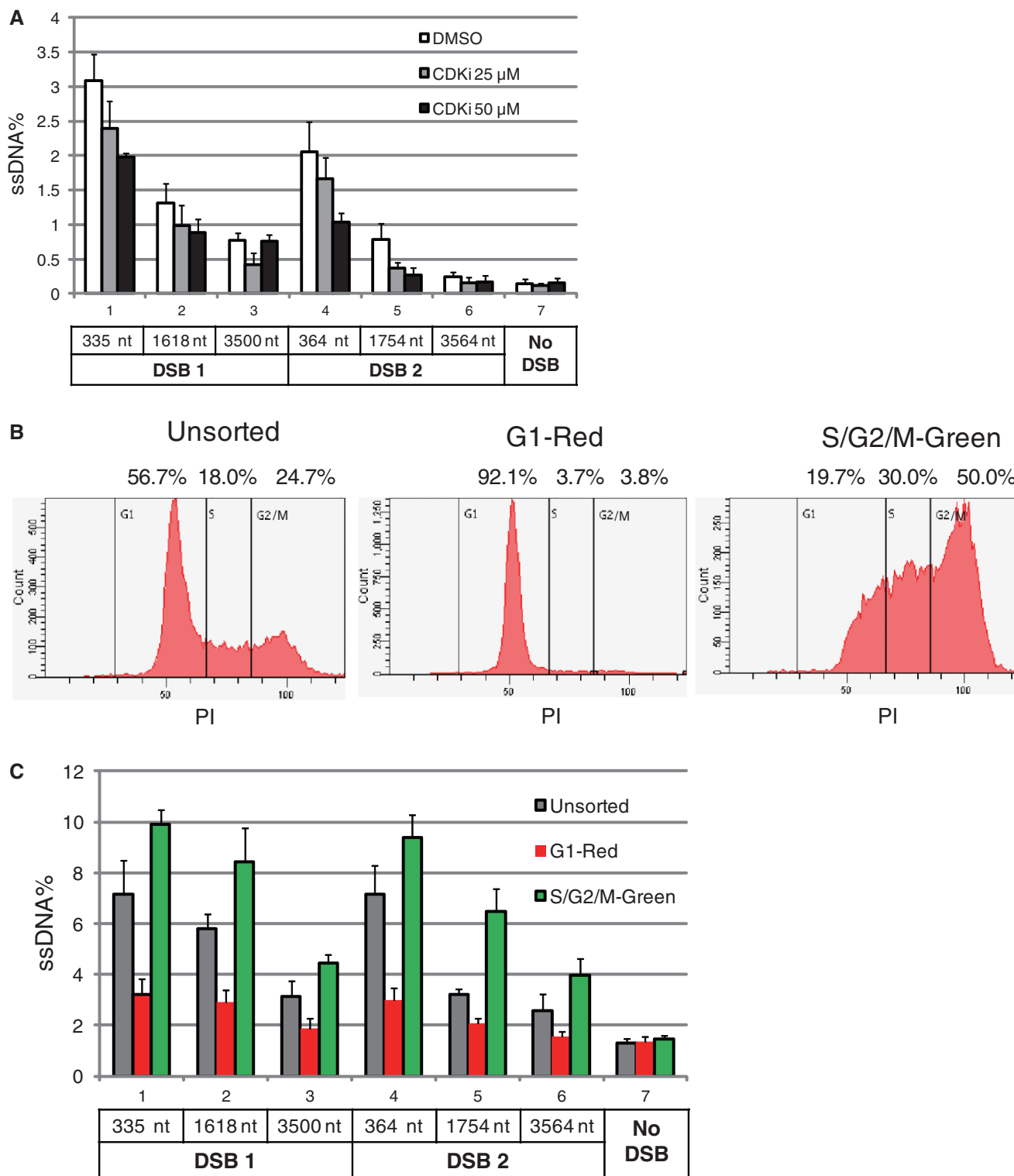


**Figure 2.** Resection of DSBs is more efficient in S/G<sub>2</sub> phases of the cell cycle. (A) ER-AsiSI U2OS cells were pretreated with 25 μM or 50 μM CDKi for 1 h, followed by induction of DSBs with 300 nM 4-OHT for 4 h and measurement of DNA resection. Error bars indicate standard deviation calculated from three experiments. See also Supplementary Figure S2. (B) ER-AsiSI 293T cells were transfected with FUCCI vectors (pRetroX-G<sub>1</sub>-Red and pRetroX-SG<sub>2</sub>M-Cyan), induced with 600 nM 4-OHT for 4 h, and sorted for G<sub>1</sub>-Red and S/G<sub>2</sub>/M-Green cells. Part of the unsorted, G<sub>1</sub>-Red and S/G<sub>2</sub>/M-Green ER-AsiSI 293T cells were stained with PI and analyzed by flow cytometry to determine the percentage of cells in G<sub>1</sub>, S and G<sub>2</sub>/M phases. (C) Measurement of DSB resection in unsorted, G<sub>1</sub>-Red and S/G<sub>2</sub>/M-Green ER-AsiSI 293T cells obtained in (B). The result is an average of three experiments with the error bars indicating standard deviation.

**The effects of known DNA repair factors on resection in human cells**

To further confirm the applicability of the resection assay, we measured resection in ER-AsiSI U2OS cells transfected with control siRNA or siRNAs directed against various genes involved in DNA repair. The MRN complex has been shown to bind to DSBs and promote resection by two independent endo/exonucleases: Exo1 and Dna2 (3). The CtIP protein also participates in this process and promotes long-range resection in conjunction with MRN (5). Resection was dramatically decreased on

knockdown of CtIP or Mre11 (Figure 3A and B; DSB% in Supplementary Table S1), consistent with previous observations (36,37). The SOSS1 ssDNA binding complex (composed of hSSB1, SOSS-A and SOSS-C) (20) was shown to be important for resection in human cells (38) and was recently shown to promote Exo1-mediated resection *in vitro* (20). Consistent with these observations, we found that depletion of SOSS1 complex using siRNA directed against the SOSS-A subunit led to reduced resection in U2OS cells, as did the depletion of Exo1 (Figure 3C and D), one of the two major

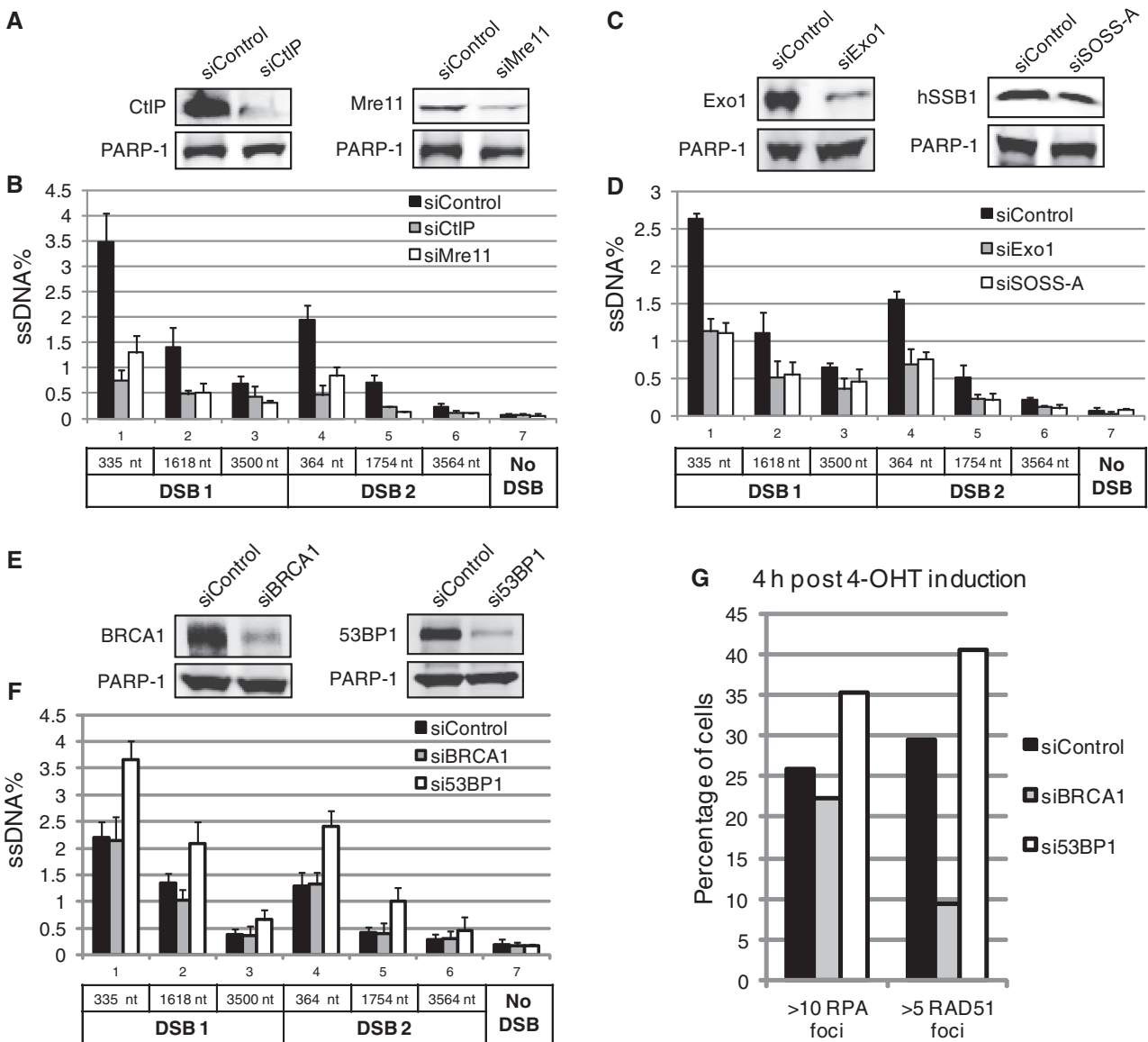


**Figure 3.** The effects of known DNA repair factors on resection. Measurement of DSB resection in ER-AsiSI U2OS cells transfected with control siRNA or siRNAs directed against CtIP or Mre11 (A and B), Exo1 or SOSS-A (C and D), BRCA1 or 53BP1 (E and F) as indicated using the assay established in Figure 1. The efficiency of knockdown was examined by western blotting and PARP-1 was used as a loading control. The efficiency of SOSS-A depletion was examined by detecting the expression of hSSB1, another subunit of the SOSS-1 complex. Error bars in (B) and (D) indicate standard deviation calculated from four experiments. The result in (F) is an average of three experiments with error bars showing standard deviation. (G) ER-AsiSI U2OS cells transfected with control siRNA or siRNAs directed against BRCA1 or 53BP1 were treated with 300nM 4-OHT for 4h, followed by immunostaining with RPA and RAD51 antibodies and counterstaining with DAPI. For RPA foci quantitation, cells with >10 RPA foci were counted (siControl N = 354; siBRCA1 N = 383; si53BP1 N = 356). For Rad51 foci quantitation, cells with >5 RAD51 foci were counted (siControl N = 494; siBRCA1 N = 583; si53BP1 N = 570).

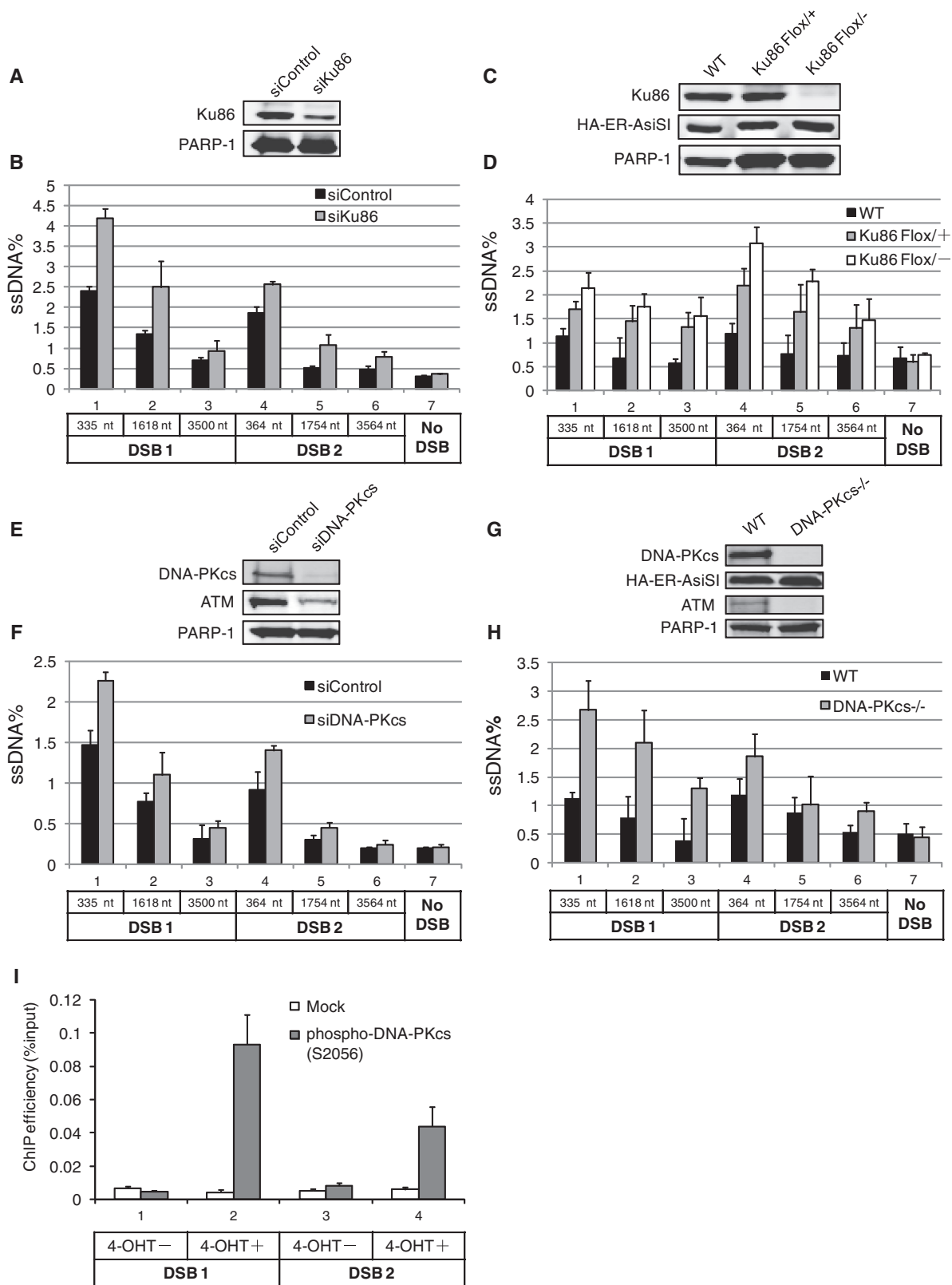


**Figure 4.** The DNA-PK enzyme blocks DSB resection. Measurement of DSB resection in ER-AsiSI U2OS cells transfected with control siRNA or siRNAs directed against Ku86 (A and B) or DNA-PKcs (E and F) as in Figure 1. (C and D) Measurement of DSB resection in WT, Ku86 heterozygous (Ku86 Flox/+) and Ku86 conditional HCT116 cells (46). WT, Ku86 Flox/+ and Ku86 Flox/- cells were transduced with ER-AsiSI retrovirus and deletion of one Ku86 allele in the Ku86 Flox/+ and Ku86 Flox/- cells was induced with Cre expression. The cells obtained were then treated with 600 nM 4-OHT for 4 h and resection was measured as in Figure 1. The result is an average of four experiments with standard deviation. The expression of Ku86 and HA-ER-AsiSI was examined by western blotting using anti-Ku86 and anti-HA antibodies, with PARP-1 as a loading control. (G and H) Measurement of DSB resection in WT and DNA-PKcs-/- HCT116 cells (47) as in (C and D). The result is an average of

(continued)

exonucleases involved in long-range resection of DSB ends. There is some variability in the ssDNA% at DSB1 and DSB2 between different experiments, which can be partially attributed to the variability in break formation by AsiSI (Supplementary Table S1).

The BRCA1 protein is a tumor suppressor that is implicated in both HR and transcriptional regulation, but the mechanistic basis of its effects are not understood. Depletion or mutation of the BRCA1 gene has been shown by many groups to reduce Rad51 foci at sites of DSBs, but whether BRCA1 directly affects resection has been controversial (39). Here we found that depletion of BRCA1 showed no significant effect on resection at either DSB1 or DSB2 (Figure 3E and F). To confirm that the depletion was sufficient to affect the functions of BRCA1 under these conditions, we also examined Rad51 foci in the U2OS cells by conventional immunofluorescence and observed a clear deficiency in Rad51 filament formation (Figure 3G). In contrast, BRCA1 depletion had little effect on RPA accumulation at damage sites in U2OS cells (Figure 3G), consistent with previous reports in chicken DT40 cells (40). These results suggest that BRCA1 promotes HR at a step later than resection of 5' strands, perhaps more similar to the mechanism of BRCA2, which binds Rad51 directly and promotes Rad51 filament formation through its mediator activity (41).

The 53BP1 protein has been shown to promote NHEJ, and is related to BRCA1 function in that the deletion of 53BP1 rescues the developmental lethality and cell cycle checkpoint defects in BRCA1-null mice and embryonic stem cells (42,43). Consistent with the view that NHEJ and HR factors compete for DSB ends, here we found that depletion of 53BP1 results in increased resection (Figure 3E and F) as previously reported (44). Depletion of 53BP1 also resulted in increased levels of RPA foci and RAD51 foci, as predicted from the increase in ssDNA (Figure 3G).

### The DNA-PK enzyme blocks DSB resection in human cells

The most highly conserved NHEJ factor is the Ku heterodimer, which is present in all organisms that use NHEJ for DNA repair (45). Ku is generally considered to be inhibitory of resection, but recent data from murine models suggest that the effect of the Ku heterodimer on resection may be minimal compared with 53BP1 (44). We used the ER-AsiSI U2OS system to address this question by depleting Ku86, a central factor in NHEJ (Figure 4A and B). These results show that even partial depletion of Ku promotes ssDNA formation by ~1.4- to 2.2-fold in U2OS cells. We also performed the resection assay in HCT116 cells engineered to conditionally delete the Ku86 gene on Cre expression (46). WT, Ku86 Flox/+ and Ku86 Flox/- HCT116 cells were transduced with

HA-ER-AsiSI retrovirus and Cre-mediated deletion of Ku86 was induced (Figure 4C and D; DSB% in Supplementary Table S1). The results confirm that the Ku heterodimer blocks resection in human cells and that a Ku86 heterozygous cell line shows haploinsufficiency for this effect.

DNA-PKcs binds to DSBs through the Ku heterodimer and is an important classical NHEJ factor. However, there is evidence showing that DNA-PKcs might be an active regulator of DSB repair pathway choice (16). To investigate whether DNA-PKcs affects DSB resection in human cells, we measured resection in AsiSI expressing U2OS cells transfected with control siRNA or siRNA directed against DNA-PKcs. As in the case of Ku depletion, knockdown of DNA-PKcs led to increased resection (Figure 4E and F). As reported previously (48), DNA-PKcs depletion also decreased the protein level of ATM, which is required for resection (5,49). The increase in DSB resection on DNA-PKcs knockdown in the background of ATM reduction suggests that DNA-PKcs strongly inhibits DSB resection *in vivo*. This conclusion was further confirmed by measuring resection in WT and DNA-PKcs-/- HCT116 cells expressing AsiSI, where DNA-PKcs deficient cells exhibited ~2.4- to 3.3-fold higher levels of resection at DSB1 and 1.2- to 1.7-fold higher levels of resection at DSB2 compared with WT cells, even though the expression of ATM was strongly reduced in DNA-PKcs-/- cells (Figure 4G and H; DSB% in Supplementary Table S1). To verify that DNA-PKcs is indeed recruited to DSB1 and DSB2, we performed ChIP and observed a clear enrichment of phospho-S2056 DNA-PKcs at both DSB sites (Figure 4I). We observed increased accumulation of DSBs on 4-OHT treatment in Ku or DNA-PKcs deficient cells (Supplementary Table S1), likely due to a failure of NHEJ, which provides more DSB ends for resection.

### DISCUSSION

In this study, we have developed a qPCR-based assay to directly measure DSB resection intermediates in human cells. In contrast to widely used assays which examine ssDNA generated by resection by indirectly detecting RPA, Rad51 or BrdU foci, the assay described here is quantitative and directly measures the level of ssDNA. In addition, it is possible to determine the length of resection from a specific DSB site using the new assay. We find that 5' strands at a DSB in human cells are degraded up to 3.5 kb from break ends, which is similar to the length of resection measured using probes that detect ssDNA formation near break sites in budding yeast (50). The AsiSI expression system used here theoretically generates ~1000 DSBs in the human genome, although not every site is cleaved on 4-OHT exposure and translocation of

#### Figure 4. Continued

four experiments with standard deviation. The expression of DNA-PKcs, ATM and HA-ER-AsiSI was examined by western blotting using anti-DNA-PKcs, anti-ATM and anti-HA antibodies, respectively, with PARP-1 as a loading control. (I) ChIP experiments were performed in ER-AsiSI U2OS cells treated or not treated with 4-OHT, using either mock antibody or antibody directed against phospho-DNA-PKcs (S2056). ChIP efficiencies (as percent of input immunoprecipitated) were measured by qPCR at 80 bp from AsiSI induced DSBs. The results are shown as mean of five independent experiments with standard deviation.

AsiSI into the nucleus (32). Approximately 150 DSBs can be actually induced by AsiSI enzyme in human cells (51). At the two AsiSI sites we have focused on, between 8 and 21% of the chromosomes incur a DSB in U2OS cells, based on qPCR across the break sites. This may be a low estimate because rapidly repaired breaks would not be detected, but it can be used to estimate the efficiency of DSB resection at sites that are cut and not immediately religated, which appears to be ~20%. This is lower than estimates of HR frequency determined from analysis of I-SceI-induced breaks in WT and repair-deficient cells, which have suggested that HR accounts for 30–40% of repair events in human cells (52), although the chromatin structure at each site as well as the cell cycle phase likely affect the efficiency of end processing.

Resection of DSBs has been shown to be efficient and extensive in the S and G<sub>2</sub> phases of the cell cycle, but limited in the G<sub>1</sub> phases (4,53,54). We also find this to be the case in the HEK293T mammalian cell system, with lower resection observed in G<sub>1</sub> cells and higher levels of the ssDNA observed in S/G<sub>2</sub>(/M) cells compared with asynchronous cultures. Here we also find measurable levels of resection in cultures that are predominantly in G<sub>1</sub> phase, however, suggesting that processing of DNA ends into ssDNA does occur, albeit less efficiently, in G<sub>1</sub> phase cells. Our survey of enzymes known to be involved in end resection (MRN, Exo1, CtIP, SOSS1), confirms that these factors are acting directly at the level of end processing and validate this method in comparison with previous results.

The Ku heterodimer and DNA-PKcs are specifically required for NHEJ, but have also been suggested to regulate end processing (13,16–19). Using the qPCR-based resection assay, we show here that the DNA-PKcs protein inhibits resection of DSB ends, the initiating step of HR. Consistent with previous reports (17,55), we find that loss of DNA-PKcs or Ku dramatically increases the efficiency of DSB resection, using both siRNA depletion and genetic deletion. This is expected considering the widely proposed competition between NHEJ and HR factors for DNA ends (17,18,56) and evidence for Ku inhibition of resection in yeast (57–60). In addition, we have investigated the role of DNA-PKcs catalytic activity in reconstituted resection assays *in vitro* and find that phosphorylation of DNA-PKcs is essential for resection when DNA-PK is present at DNA ends (61). We conclude that the DNA-PKcs protein inhibits resection, but this inhibition can be overcome by DNA-PKcs phosphorylation that promotes dissociation of DNA-PKcs kinase from DSB ends and recruitment of resection enzymes.

Using the AsiSI system shown here we also measured the levels of DSBs and observed increased accumulation of unresolved breaks on 4-OHT treatment in Ku or DNA-PKcs deficient cells (Supplementary Table S1), likely due to a failure of NHEJ repair. Notably, even though depletion of 53BP1 and depletion of Ku or DNA-PKcs have similar stimulatory effects on resection, only depletion of the DNA-PK holoenzyme components increases the apparent accumulation of unresolved DSBs (Supplementary Table S1). This suggests that 53BP1 is not involved in the initial fast process of religation but

may affect pathway choice for the subset of breaks that goes through resection and HR.

Recent observations showing that 53BP1 deletion rescues many of the defects seen in BRCA1-deficient cells (42,43) suggest that BRCA1 function must be to antagonize 53BP1 in some way. Yet here we demonstrate that BRCA1 depletion has minimal effect on end processing under conditions where Rad51 filament formation is clearly compromised. It is possible that Rad51 filaments in BRCA1-depleted cells are qualitatively different from those in WT cells, leading to differences in foci intensity, or perhaps BRCA1 affects resection at some genomic sites more than others. From the data we have collected, however, we suggest that the function of BRCA1 may be to promote Rad51 filament formation, whereas 53BP1 is antagonizing the end resection process directly.

In conclusion, we have developed a method to analyze the levels of ssDNA quantitatively in mammalian cells and have demonstrated the validity of this method. Here we have used it in the context of site-specific DSBs to measure end resection, but in theory this method can be used to quantitate ssDNA intermediates in any genomic context. Direct measurement of DSBs has obvious advantages over foci-based methods in that quantitative analysis of the actual resection products can be performed; however, we note that this is limited by the requirement for sequence specificity of the cut site. Other methods such as RPA ChIP-Seq have also been used to address the need for resection assays at random or unknown DNA damage sites in the mammalian genome (62,63). A combination of these methods may be necessary to quantitatively measure ssDNA at nuclease-accessible as well as inaccessible sites and to assess resection efficiency in response to different types of DNA damage.

## SUPPLEMENTARY DATA

Supplementary Data are available at NAR Online.

## ACKNOWLEDGEMENTS

We thank Dr Eric Hendrickson for Ku conditional and DNA-PKcs null HCT116 cells. We are grateful to members of the Paull laboratory and to Dr Kyle Miller for helpful comments.

## FUNDING

Cancer Prevention and Research Institute of Texas [RP110465-P4 toward work in the Paull laboratory]. Funding for open access charge: HHMI.

*Conflict of interest statement.* None declared.

## REFERENCES

1. Ciccia, A. and Elledge, S.J. (2010) The DNA damage response: making it safe to play with knives. *Mol. Cell*, **40**, 179–204.
2. Trovesi, C., Manfrini, N., Falcattoni, M. and Longhese, M.P. (2013) Regulation of the DNA damage response by cyclin-dependent kinases. *J. Mol. Biol.*, **425**, 4756–4766.

3. Mimitou, E.P. and Symington, L.S. (2009) DNA end resection: many nucleases make light work. *DNA Repair*, **8**, 983–995.
4. Huertas, P. and Jackson, S.P. (2009) Human CtIP mediates cell cycle control of DNA end resection and double strand break repair. *J. Biol. Chem.*, **284**, 9558–9565.
5. You, Z., Shi, L.Z., Zhu, Q., Wu, P., Zhang, Y.W., Basilio, A., Tonnu, N., Verma, I.M., Berns, M.W. and Hunter, T. (2009) CtIP links DNA double-strand break sensing to resection. *Mol. Cell*, **36**, 954–969.
6. Morrison, C., Sonoda, E., Takao, N., Shinohara, A., Yamamoto, K. and Takeda, S. (2000) The controlling role of ATM in homologous recombinational repair of DNA damage. *EMBO J.*, **19**, 463–471.
7. Kuhne, M., Riballo, E., Rief, N., Rothkamm, K., Jeggo, P.A. and Lobrich, M. (2004) A double-strand break repair defect in ATM-deficient cells contributes to radiosensitivity. *Cancer Res.*, **64**, 500–508.
8. Wang, C. and Lees-Miller, S.P. (2013) Detection and repair of ionizing radiation-induced DNA double strand breaks: new developments in nonhomologous end joining. *Int. J. Radiat. Oncol. Biol. Phys.*, **86**, 440–449.
9. Merkle, D., Douglas, P., Moorhead, G.B., Leonenko, Z., Yu, Y., Cramb, D., Bazett-Jones, D.P. and Lees-Miller, S.P. (2002) The DNA-dependent protein kinase interacts with DNA to form a protein-DNA complex that is disrupted by phosphorylation. *Biochemistry*, **41**, 12706–12714.
10. Dobbs, T.A., Tainer, J.A. and Lees-Miller, S.P. (2010) A structural model for regulation of NHEJ by DNA-PKcs autophosphorylation. *DNA Repair*, **9**, 1307–1314.
11. Ding, Q., Reddy, Y.V., Wang, W., Woods, T., Douglas, P., Ramsden, D.A., Lees-Miller, S.P. and Meek, K. (2003) Autophosphorylation of the catalytic subunit of the DNA-dependent protein kinase is required for efficient end processing during DNA double-strand break repair. *Mol. Cell Biol.*, **23**, 5836–5848.
12. Reddy, Y.V., Ding, Q., Lees-Miller, S.P., Meek, K. and Ramsden, D.A. (2004) Non-homologous end joining requires that the DNA-PK complex undergo an autophosphorylation-dependent rearrangement at DNA ends. *J. Biol. Chem.*, **279**, 39408–39413.
13. Shibata, A., Conrad, S., Birraux, J., Geuting, V., Barton, O., Ismail, A., Kakarougkas, A., Meek, K., Taucher-Scholz, G., Lobrich, M. *et al.* (2011) Factors determining DNA double-strand break repair pathway choice in G2 phase. *EMBO J.*, **30**, 1079–1092.
14. Meek, K., Douglas, P., Cui, X., Ding, Q. and Lees-Miller, S.P. (2007) trans Autophosphorylation at DNA-dependent protein kinase's two major autophosphorylation site clusters facilitates end processing but not end joining. *Mol. Cell Biol.*, **27**, 3881–3890.
15. Chen, B.P., Uematsu, N., Kobayashi, J., Lerenthal, Y., Krempler, A., Yajima, H., Lobrich, M., Shiloh, Y. and Chen, D.J. (2007) Ataxia telangiectasia mutated (ATM) is essential for DNA-PKcs phosphorylations at the Thr-2609 cluster upon DNA double strand break. *J. Biol. Chem.*, **282**, 6582–6587.
16. Cui, X., Yu, Y., Gupta, S., Cho, Y.M., Lees-Miller, S.P. and Meek, K. (2005) Autophosphorylation of DNA-dependent protein kinase regulates DNA end processing and may also alter double-strand break repair pathway choice. *Mol. Cell Biol.*, **25**, 10842–10852.
17. Neal, J.A., Dang, V., Douglas, P., Wold, M.S., Lees-Miller, S.P. and Meek, K. (2011) Inhibition of homologous recombination by DNA-dependent protein kinase requires kinase activity, is titratable, and is modulated by autophosphorylation. *Mol. Cell Biol.*, **31**, 1719–1733.
18. Allen, C., Halbrook, J. and Nickoloff, J.A. (2003) Interactive competition between homologous recombination and non-homologous end joining. *Mol. Cancer Res.*, **1**, 913–920.
19. Convery, E., Shin, E.K., Ding, Q., Wang, W., Douglas, P., Davis, L.S., Nickoloff, J.A., Lees-Miller, S.P. and Meek, K. (2005) Inhibition of homologous recombination by variants of the catalytic subunit of the DNA-dependent protein kinase (DNA-PKcs). *Proc. Natl Acad. Sci. USA*, **102**, 1345–1350.
20. Yang, S.H., Zhou, R., Campbell, J., Chen, J., Ha, T. and Paull, T.T. (2013) The SOSS1 single-stranded DNA binding complex promotes DNA end resection in concert with Exo1. *EMBO J.*, **32**, 126–139.
21. Shim, E.Y., Chung, W.H., Nicolette, M.L., Zhang, Y., Davis, M., Zhu, Z., Paull, T.T., Ira, G. and Lee, S.E. (2010) Saccharomyces cerevisiae Mre11/Rad50/Xrs2 and Ku proteins regulate association of Exo1 and Dna2 with DNA breaks. *EMBO J.*, **29**, 3370–3380.
22. Sakaue-Sawano, A., Kurokawa, H., Morimura, T., Hanyu, A., Hama, H., Osawa, H., Kashiwagi, S., Fukami, K., Miyata, T., Miyoshi, H. *et al.* (2008) Visualizing spatiotemporal dynamics of multicellular cell-cycle progression. *Cell*, **132**, 487–498.
23. Zierhut, C. and Diffley, J.F. (2008) Break dosage, cell cycle stage and DNA replication influence DNA double strand break response. *EMBO J.*, **27**, 1875–1885.
24. Nicolette, M.L., Lee, K., Guo, Z., Rani, M., Chow, J.M., Lee, S.E. and Paull, T.T. (2010) Mre11-Rad50-Xrs2 and Sae2 promote 5' strand resection of DNA double-strand breaks. *Nat. Struct. Mol. Biol.*, **17**, 1478–1485.
25. Cejka, P., Cannavo, E., Polczek, P., Masuda-Sasa, T., Pokharel, S., Campbell, J.L. and Kowalczykowski, S.C. (2010) DNA end resection by Dna2-Sgs1-RPA and its stimulation by Top3-Rmi1 and Mre11-Rad50-Xrs2. *Nature*, **467**, 112–116.
26. Quennet, P., Beucher, A., Barton, O., Takeda, S. and Lobrich, M. (2011) CtIP and MRN promote non-homologous end-joining of etoposide-induced DNA double-strand breaks in G1. *Nucleic Acids Res.*, **39**, 2144–2152.
27. Huang, J., Gong, Z., Ghosal, G. and Chen, J. (2009) SOSS complexes participate in the maintenance of genomic stability. *Mol. Cell*, **35**, 384–393.
28. Bolderson, E., Tomimatsu, N., Richard, D.J., Boucher, D., Kumar, R., Pandita, T.K., Burma, S. and Khanna, K.K. (2010) Phosphorylation of Exo1 modulates homologous recombination repair of DNA double-strand breaks. *Nucleic Acids Res.*, **38**, 1821–1831.
29. Peng, Y., Zhang, Q., Nagasawa, H., Okayasu, R., Liber, H.L. and Bedford, J.S. (2002) Silencing expression of the catalytic subunit of DNA-dependent protein kinase by small interfering RNA sensitizes human cells for radiation-induced chromosome damage, cell killing, and mutation. *Cancer Res.*, **62**, 6400–6404.
30. Lou, Z., Chini, C.C., Minter-Dykhouse, K. and Chen, J. (2003) Mediator of DNA damage checkpoint protein 1 regulates BRCA1 localization and phosphorylation in DNA damage checkpoint control. *J. Biol. Chem.*, **278**, 13599–13602.
31. Kachirskaja, I., Shi, X., Yamaguchi, H., Tanoue, K., Wen, H., Wang, E.W., Appella, E. and Gozani, O. (2008) Role for 53BP1 Tudor domain recognition of p53 dimethylated at lysine 382 in DNA damage signaling. *J. Biol. Chem.*, **283**, 34660–34666.
32. Iacovoni, J.S., Caron, P., Lassadi, I., Nicolas, E., Massip, L., Trouche, D. and Legube, G. (2010) High-resolution profiling of gammaH2AX around DNA double strand breaks in the mammalian genome. *EMBO J.*, **29**, 1446–1457.
33. Stenerlow, B., Karlsson, K.H., Cooper, B. and Rydberg, B. (2003) Measurement of prompt DNA double-strand breaks in mammalian cells without including heat-labile sites: results for cells deficient in nonhomologous end joining. *Radiat. Res.*, **159**, 502–510.
34. Miller, K.M., Tjeertes, J.V., Coates, J., Legube, G., Polo, S.E., Britton, S. and Jackson, S.P. (2010) Human HDAC1 and HDAC2 function in the DNA-damage response to promote DNA nonhomologous end-joining. *Nat. Struct. Mol. Biol.*, **17**, 1144–1151.
35. Alessi, F., Quarta, S., Savio, M., Riva, F., Rossi, L., Stivala, L.A., Scovassi, A.I., Meijer, L. and Prosperi, E. (1998) The cyclin-dependent kinase inhibitors olomoucine and roscovitine arrest human fibroblasts in G1 phase by specific inhibition of CDK2 kinase activity. *Exp. Cell Res.*, **245**, 8–18.
36. Yamaguchi-Iwai, Y., Sonoda, E., Sasaki, M.S., Morrison, C., Haraguchi, T., Hiraoka, Y., Yamashita, Y.M., Yagi, T., Takata, M., Price, C. *et al.* (1999) Mre11 is essential for the maintenance of chromosomal DNA in vertebrate cells. *EMBO J.*, **18**, 6619–6629.
37. Sartori, A.A., Lukas, C., Coates, J., Mistrik, M., Fu, S., Bartek, J., Baer, R., Lukas, J. and Jackson, S.P. (2007) Human CtIP promotes DNA end resection. *Nature*, **450**, 509–514.

38. Richard, D.J., Bolderson, E., Cubeddu, L., Wadsworth, R.I., Savage, K., Sharma, G.G., Nicolette, M.L., Tsvetanov, S., McIlwraith, M.J., Pandita, R.K. *et al.* (2008) Single-stranded DNA-binding protein hSSB1 is critical for genomic stability. *Nature*, **453**, 677–681.
39. Symington, L.S. and Gautier, J. (2011) Double-strand break end resection and repair pathway choice. *Annu. Rev. Genet.*, **45**, 247–271.
40. Nakamura, K., Kogame, T., Oshiumi, H., Shinohara, A., Sumitomo, Y., Agama, K., Pommier, Y., Tsutsui, K.M., Tsutsui, K., Hartsuiker, E. *et al.* (2010) Collaborative action of Brc1 and CtIP in elimination of covalent modifications from double-strand breaks to facilitate subsequent break repair. *PLoS Genet.*, **6**, e1000828.
41. Holloman, W.K. (2011) Unraveling the mechanism of BRCA2 in homologous recombination. *Nat. Struct. Mol. Biol.*, **18**, 748–754.
42. Bouwman, P., Aly, A., Escandell, J.M., Pieterse, M., Bartkova, J., van der Gulden, H., Hiddingh, S., Thanasoula, M., Kulkarni, A., Yang, Q. *et al.* (2010) 53BP1 loss rescues BRCA1 deficiency and is associated with triple-negative and BRCA-mutated breast cancers. *Nat. Struct. Mol. Biol.*, **17**, 688–695.
43. Bunting, S.F., Callen, E., Wong, N., Chen, H.T., Polato, F., Gunn, A., Bothmer, A., Feldhahn, N., Fernandez-Capetillo, O., Cao, L. *et al.* (2010) 53BP1 inhibits homologous recombination in Brc1-deficient cells by blocking resection of DNA breaks. *Cell*, **141**, 243–254.
44. Bunting, S.F., Callen, E., Kozak, M.L., Kim, J.M., Wong, N., Lopez-Contreras, A.J., Ludwig, T., Baer, R., Faryabi, R.B., Malhowski, A. *et al.* (2012) BRCA1 functions independently of homologous recombination in DNA interstrand crosslink repair. *Mol. Cell*, **46**, 125–135.
45. Hiom, K. (2003) DNA repair: bacteria join in. *Curr. Biol.*, **13**, R28–R30.
46. Fattah, F., Lee, E.H., Weisensel, N., Wang, Y., Lichter, N. and Hendrickson, E.A. (2010) Ku regulates the non-homologous end joining pathway choice of DNA double-strand break repair in human somatic cells. *PLoS Genet.*, **6**, e1000855.
47. Ruis, B.L., Fattah, K.R. and Hendrickson, E.A. (2008) The catalytic subunit of DNA-dependent protein kinase regulates proliferation, telomere length, and genomic stability in human somatic cells. *Mol. Cell Biol.*, **28**, 6182–6195.
48. Peng, Y., Woods, R.G., Beamish, H., Ye, R., Lees-Miller, S.P., Lavin, M.F. and Bedford, J.S. (2005) Deficiency in the catalytic subunit of DNA-dependent protein kinase causes down-regulation of ATM. *Cancer Res.*, **65**, 1670–1677.
49. Jazayeri, A., Falck, J., Lukas, C., Bartek, J., Smith, G.C., Lukas, J. and Jackson, S.P. (2006) ATM- and cell cycle-dependent regulation of ATR in response to DNA double-strand breaks. *Nat. Cell Biol.*, **8**, 37–45.
50. Chung, W.H., Zhu, Z., Papusha, A., Malkova, A. and Ira, G. (2010) Defective resection at DNA double-strand breaks leads to de novo telomere formation and enhances gene targeting. *PLoS Genet.*, **6**, e1000948.
51. Massip, L., Caron, P., Iacovoni, J.S., Trouche, D. and Legube, G. (2010) Deciphering the chromatin landscape induced around DNA double strand breaks. *Cell Cycle*, **9**, 2963–2972.
52. Johnson, R.D. and Jasin, M. (2001) Double-strand-break-induced homologous recombination in mammalian cells. *Biochem. Soc. Trans.*, **29**, 196–201.
53. Aylon, Y., Liefshitz, B. and Kupiec, M. (2004) The CDK regulates repair of double-strand breaks by homologous recombination during the cell cycle. *EMBO J.*, **23**, 4868–4875.
54. Ira, G., Pellicoli, A., Balijja, A., Wang, X., Fiorani, S., Carotenuto, W., Liberi, G., Bressan, D., Wan, L., Hollingsworth, N.M. *et al.* (2004) DNA end resection, homologous recombination and DNA damage checkpoint activation require CDK1. *Nature*, **431**, 1011–1017.
55. Allen, C., Kurimasa, A., Brenneman, M.A., Chen, D.J. and Nickoloff, J.A. (2002) DNA-dependent protein kinase suppresses double-strand break-induced and spontaneous homologous recombination. *Proc. Natl Acad. Sci. USA*, **99**, 3758–3763.
56. Shrivastav, M., De Haro, L.P. and Nickoloff, J.A. (2008) Regulation of DNA double-strand break repair pathway choice. *Cell Res.*, **18**, 134–147.
57. Clerici, M., Mantiero, D., Guerini, I., Lucchini, G. and Longhese, M.P. (2008) The Yku70-Yku80 complex contributes to regulate double-strand break processing and checkpoint activation during the cell cycle. *EMBO Rep.*, **9**, 810–818.
58. Krishna, S., Wagener, B.M., Liu, H.P., Lo, Y.C., Sterk, R., Petrini, J.H. and Nickoloff, J.A. (2007) Mre11 and Ku regulation of double-strand break repair by gene conversion and break-induced replication. *DNA Repair*, **6**, 797–808.
59. Lee, S.E., Moore, J.K., Holmes, A., Umez, K., Kolodner, R.D. and Haber, J.E. (1998) Saccharomyces Ku70, mre11/rad50 and RPA proteins regulate adaptation to G2/M arrest after DNA damage. *Cell*, **94**, 399–409.
60. Zhang, Y., Hefferin, M.L., Chen, L., Shim, E.Y., Tseng, H.M., Kwon, Y., Sung, P., Lee, S.E. and Tomkinson, A.E. (2007) Role of Dnl4-Lif1 in nonhomologous end-joining repair complex assembly and suppression of homologous recombination. *Nat. Struct. Mol. Biol.*, **14**, 639–646.
61. Zhou, Y. and Paull, T.T. (2013) DNA-dependent Protein Kinase regulates DNA end resection in concert with Mre11-Rad50-Nbs1 (MRN) and Ataxia-Telangiectasia-Mutated (ATM). *J. Biol. Chem.*, **288**, 37112–37125.
62. Yamane, A., Resch, W., Kuo, N., Kuchen, S., Li, Z., Sun, H.W., Robbiani, D.F., McBride, K., Nussenzweig, M.C. and Casellas, R. (2011) Deep-sequencing identification of the genomic targets of the cytidine deaminase AID and its cofactor RPA in B lymphocytes. *Nat. Immunol.*, **12**, 62–69.
63. Yamane, A., Robbiani, D.F., Resch, W., Bothmer, A., Nakahashi, H., Oliveira, T., Rommel, P.C., Brown, E.J., Nussenzweig, A., Nussenzweig, M.C. *et al.* (2013) RPA accumulation during class switch recombination represents 5'-3' DNA-end resection during the S-G2/M phase of the cell cycle. *Cell Rep.*, **3**, 138–147.